HHS Public Access

Author manuscript

Nat Med. Author manuscript; available in PMC 2018 February 14.

Published in final edited form as:

Nat Med. 2017 September ; 23(9): 1063–1071. doi:10.1038/nm.4378.

Prostate cancer-associated SPOP mutations confer resistance to BET inhibitors through stabilization of BRD4

Xiangpeng Dai[1,*], **Wenjian Gan**[1,*], **Xiaoning Li**[1,2,*], **Shangqian Wang**[3], **Wei Zhang**[4,11], **Ling Huang**[5], **Shengwu Liu**[6], **Qing Zhong**[7], **Jianping Guo**[1], **Jinfang Zhang**[1], **Ting Chen**[6], **Kouhei Shimizu**[1], **Francisco Beca**[1], **Mirjam Blattner**[10], **Divya Vasudevan**[10], **Dennis L. Buckley**[6], **Jun Qi**[6], **Lorenz Buser**[7], **Pengda Liu**[1,12], **Hiroyuki Inuzuka**[1], **Andrew H. Beck**[1], **Liewei Wang**[13], **Peter J. Wild**[7], **Levi A. Garraway**[8], **Mark A. Rubin**[9], **Christopher E. Barbieri**[10], **Kwok-Kin Wong**[6], **Senthil K. Muthuswamy**[5], **Jiaoti Huang**[4], **Yu Chen**[3], **James E. Bradner**[6], and **Wenyi Wei**[1,14]

[1]Department of Pathology, Beth Israel Deaconess Medical Center, Harvard Medical School, Boston, MA 02115, USA [2]Department of Pathophysiology, Basic Medical College, Jilin University, Changchun, 130021, China [3]Human Oncology and Pathogenesis Program, Memorial Sloan Kettering Cancer Center, New York, NY 10065, USA [4]Department of Pathology, Duke University School of Medicine, Durham, NC 27710, USA [5]Cancer Research Institute, Beth Israel Deaconess Medical Center, Harvard Medical School, Boston, MA 02115, USA [6]Department of Medical Oncology, Dana-Farber Cancer Institute, Harvard Medical School, Boston, MA 02215, USA. Department of Medicine, Harvard Medical School, Boston, MA 02215, USA [7]Institute of Pathology and Molecular Pathology, University Hospital Zurich, Zurich, ZH 8091, Switzerland [8]Department of Medical Oncology, Dana-Farber Cancer Institute, Boston, MA 02215, USA. Broad Institute of MIT and Harvard, Cambridge, MA 02142, USA [9]Institute for Precision Medicine and Department of Pathology and Laboratory Medicine, Weill Cornell Medical College, New York, NY 10065, USA; Sandra and Edward Meyer Cancer Center, Weill Cornell Medical College, New York, NY 10065, USA [10]Department of Urology, Sandra and Edward Meyer Cancer Center, Weill Cornell Medical College, New York, NY 10065, USA [11]Department of Pathology, Beijing Hospital, National Center of Gerontology, Beijing 100730, P. R. China [13]Department of Molecular Pharmacology and Experimental Therapeutics, Mayo Clinic, Rochester, MN 55905, USA

[14]Correspondence should be addressed to Dr. Wenyi Wei, wwei2@bidmc.harvard.edu.
[12]Present address: Department of Biochemistry and Biophysics, Lineberger Comprehensive Cancer Center, University of North Carolina at Chapel Hill, Chapel Hill, NC 27599.
*These authors contributed equally to this work.

AUTHOR CONTRIBUTIONS

X.D., W.G. and X.L. designed and performed most of the experiments with assistance from J.G., J.Z., K.S., H.I., P.L., L.W. and L.A.G. W.Z., Q.Z., L.B., P.J.W. and J.H. performed IHC. X.D., W.G., J.G., J. Z., S.L., T.C., and K.-K.W. performed the Xenograft assay. L.H., S.W., S.K.M. and Y.C. performed the 3D cell culture assays. F.B. and A.H.B. performed the bioinformatics analysis. D.V., M.B., M.A.R. and C.E.B. performed assays with transgenic mice. D.L.B., J.Q. and J.E.B. provided BET inhibitors and performed related drug treatment. W.W. designed the experiments and supervised the study. W.G. X.D. and W.W. wrote the manuscript. All authors commented on the manuscript.

COMPETING FINANCIAL INTERESTS

The authors declare no competing financial interests.

Abstract

The bromodomain and extra-terminal (BET) family of proteins, comprised of four members including BRD2, BRD3, BRD4 and the testis-specific isoform BRDT, largely function as transcriptional co-activators [1–3] and play critical roles in various cellular processes, including cell cycle, apoptosis, migration and invasion [4,5]. As such, BET proteins enhance the oncogenic functions of major cancer drivers by either elevating their expression such as c-Myc in leukemia [6,7] or by promoting transcriptional activities of oncogenic factors such as AR and ERG in the prostate cancer setting [8]. Pathologically, BET proteins are frequently overexpressed and clinically linked to various types of human cancers [5,9,10], therefore pursued as attractive therapeutic targets for selective inhibition in patients. To this end, a number of bromodomain inhibitors, including JQ1 and I-BET, have been developed [11,12] and shown promising outcomes in early clinical trials. Despite resistance to BET inhibitor has been documented in pre-clinical models [13–15] the molecular mechanisms underlying acquired resistance are largely unknown. Here, we report that Cullin 3^{SPOP} earmarks BET proteins including BRD2, BRD3 and BRD4 for ubiquitination-mediated degradation. Pathologically, prostate cancer-associated SPOP mutants fail to interact with and promote the destruction of BET proteins, leading to their elevated abundance in *SPOP*-deficient prostate cancer. As a result, prostate cancer cells and prostate cancer patient-derived organoids harboring *SPOP* mutations are more resistant to BET inhibitor-induced cell growth arrest and apoptosis. Therefore, our results elucidate the tumor suppressor role of SPOP in prostate cancer by negatively controlling BET protein stability, and also provide a molecular mechanism for BET inhibitor resistance in prostate cancer patients bearing *SPOP* mutations.

Given that resistance to targeted therapies is frequently associated with accumulation of the targeted protein [16–18], it is crucial to understand how BET protein stability is regulated and whether deregulation of BET protein abundance contributes to cellular resistance to BET inhibitors. To this end, we observed that in 22Rv1 prostate cancer cells, treatment with the proteasome inhibitor, MG132, and the Cullin-RING ubiquitin ligases inhibitor, MLN4924, led to a significant increase in endogenous BRD4 abundance, indicating the involvement of the Cullin-based ligase(s) in regulating BRD4 protein stability (Fig. 1a). In support of this notion, we found that BRD4 primarily interacted with Cullin 3 (Cul 3), and to a much lesser extent, Cullin 1 (Cul 1), but not other members of the Cullin family (Fig. 1b). Consistently, ectopic expression of Cul 3 decreased the protein abundance of BRD4 in a dose-dependent manner (Supplementary Fig. 1a). On the other hand, depletion of endogenous *Cul 3,* but not *Cul 1, Cul 4A or Cul 4B,* led to a marked elevation of endogenous BRD2, BRD3 and BRD4 protein levels (Fig. 1c and Supplementary Fig. 1b, c), largely by extending protein half-life (Supplementary Fig. 1d, e). These data suggest that Cul 3-based ligase(s) might be responsible for governing BET protein stability.

Previous studies demonstrated that Cul 3 recruits downstream ubiquitin substrates through interaction with BTB-domain-containing proteins as substrate-specific adaptors, including KLHL20, Keap1 and SPOP [19]. Interestingly, we found that only SPOP, but not other Cul 3-based BTB-domain-containing adaptor proteins we examined, specifically interacts with BET proteins (Fig. 1d and Supplementary Fig. 1f–i). Notably, SPOP, but not Keap1 nor hCOP1, a Cullin 4-based E3 ligase substrate adaptor protein [20], promoted BET protein degradation in a dose-dependent manner (Fig. 1e and Supplementary Fig. 1j–l). More

importantly, SPOP-mediated degradation of BRD4 could be efficiently blocked by MG132 (Supplementary Fig. 1m), indicating that SPOP regulates BRD4 abundance through the ubiquitin-proteasome pathway. In keeping with these findings, depletion of endogenous *SPOP* by shRNAs or CRISPR-mediated knockout in multiple prostate cancer cell lines or MEFs led to a marked increase in the protein abundance of BET proteins as well as other identified SPOP substrates, including DEK, AR and ERG (Fig. 1f–h and Supplementary Fig. 1n, o). Moreover, we found that SPOP, but not other Cul 3-based adaptor proteins we examined or hCOP1, specifically promotes BET protein ubiquitination in cells (Fig. 1i and Supplementary Fig. 1p, q). Importantly, BRD4 mRNA levels were minimally changed (Supplementary Fig. 1r), while the half-life of BRD4 was significantly extended in *SPOP*-depleted cells (Fig. 1j, k and Supplementary Fig. 1s, t). These results collectively suggest that the BET family of proteins, including BRD2, BRD3 and BRD4, are potential downstream substrates of the Cul 3^{SPOP} E3 ubiquitin ligase.

Next, we sought to understand the biological effects of SPOP in governing BRD4 stability. BRD4 has previously shown to play a critical role in cell proliferation, migration and invasion by directly associating with positive transcription elongation factor b (P-TEFb) [21,22] or interacting with DNA-specific transcription factors, including p53, c-Myc, AR and ERG [8,23]. Consistent with a critical role for BRD4 to serve as transcriptional co-activator for AR and ERG [8,23], we first confirmed that BET proteins bind both endogenous and ectopically expressed AR and ERG in cells (Supplementary Fig. 2a–c). Moreover, depletion of *SPOP* significantly up-regulated the mRNA levels of AR and ERG target genes largely in a BRD4-dependent manner in prostate cancer cells (Supplementary Fig. 2d–g). Consistently, the mRNA levels of AR and ERG target genes were significantly decreased in *BRD4* knockout or JQ1 treated C4-2 cells (Supplementary Fig. 2h–l). Importantly, stable expression of AR or ERG in *BRD4* knockout cells failed to restore the expression of their downstream target genes (Supplementary Fig. 2m–p), indicating that BRD4 plays a critical role as a co-activator in controlling AR and ERG transcriptional activity. As a result, we observed that compared with control (shScr), depletion of *BRD4* led to significant inhibition of cell proliferation (Fig. 1l), colony formation (Fig. 1m), anchorage independent growth (Fig. 1n) and migration (Fig. 1o–q). In contrast, depletion of endogenous *SPOP* led to a significant elevation of BRD4 protein abundance (Fig. 1o and Supplementary Fig. 2g), and a BRD4-dependent increase in cell proliferation (Fig. 1l and Supplementary Fig. 2q, r), colony formation (Fig. 1m), anchorage independent growth (Fig. 1n) and migration (Fig. 1o–q). Moreover, simultaneous depletion of endogenous *BRD4* with *AR* or *ERG* displayed similar proliferation rate or cellular migration ability compared to individual depletion of either gene (Fig. 1o–q and Supplementary Fig. 2s–v). Altogether, these data suggest that SPOP suppresses prostate cancer progression largely by targeting BRD4 for ubiquitination and subsequent destruction, which results in an attenuation of BRD4-dependent AR/ERG signaling in prostate cancer (Supplementary Fig. 2w).

SPOP is a member of the MATH-BTB protein family containing an N-terminal MATH domain and a C-terminal BTB domain [24]. The MATH domain is responsible for substrate recognition and interaction, while the BTB domain binds Cul 3 forming the functional E3 ubiquitin ligase complex. Recent genome-wide sequencing studies have revealed that *SPOP* is the most frequently mutated gene (up to 10%) in prostate cancers [25,26]. Interestingly, all

SPOP somatic mutations identified in prostate cancers including Y87C, F102C, W131G and F133V, occur in the MATH domain (Fig. 2a) and play a dominant-negative role in substrate binding and degradation [27]. In keeping with previous reports [24,28], we found that deletion of the MATH domain abolishes SPOP interaction with BRD4 (Fig. 2b) and both the MATH domain and BTB domain are required for SPOP-mediated BRD4 ubiquitination and degradation (Fig. 2c and Supplementary Fig. 3a). Next, we sought to explore whether prostate cancer-associated *SPOP* mutations affect BRD4 stability. Notably, all mutants we examined failed to interact with BRD2, BRD3 and BRD4 in HEK293 and prostate cancer cells (Fig. 2d and Supplementary Fig. 3b–d), and were thereby deficient in promoting the degradation of BET proteins (Fig. 2e and Supplementary Fig. 3e–h). Moreover, ectopic expression of SPOP-WT, but not the SPOP mutants, significantly shortened the half-life of BRD4 (Fig. 2f and Supplementary Fig. 3i) and promoted BET proteins ubiquitination in cells (Fig. 2g and Supplementary Fig. 3j, k).

In keeping with these findings, induced expression of SPOP-F133V in the prostate of mice also exhibited elevation in protein abundance of BRD2, BRD3 and BRD4 (Supplementary Fig. 3l). Consistently, compared to ectopic expression of SPOP-WT, stable expression of SPOP mutants in prostate cancer cells increased mRNA levels of ERG downstream target genes (Supplementary Fig. 3m). As a result, cells expressing prostate cancer-derived SPOP mutants displayed enhanced colony formation ability in monolayer culture and increased growth on three-dimensional extracellular matrix compared with cells expressing SPOP-WT (Fig. 2h and Supplementary Fig. 4a), a process that can be largely abolished by depleting endogenous *BRD4* (Fig. 2i and Supplementary Fig. 4b). Consistently, depletion of *BRD4* by CRISPR-mediated knockout or shRNA in cells expressing SPOP mutations significantly retarded tumor growth in xenograft mouse models (Fig. 2j–l and Supplementary Fig. 4c–k). Taken together, these results suggest a physiological role for BRD4 in promoting cell proliferation and *in vivo* prostate tumorigenesis downstream prostate cancer-specific *SPOP* mutations.

To further evaluate the clinical significance of SPOP-mediated BRD4 degradation, we performed BRD4 immunohistochemistry (IHC) staining in 66 SPOP-WT and 12 SPOP-mutation prostate cancer patient samples [28] and observed an inverse correlation between SPOP mutation status and BRD4 expression (Fig. 2m, n). Moreover, BRD4 expression was gradually increased from samples [29] of benign prostatic hyperplasia (BPH) to castration-resistant prostate cancer (CRPC) and significantly associated with shorter overall, disease-specific and PSA recurrence-free survival after radical prostatectomy in primary prostate cancer (Supplementary Fig. 5a–c). Furthermore, using two class paired significance analysis of microarrays in normal-tumor pairs to compute transcriptome-wide differential test statistics (d-statistics), we found a strong correlation (Rho=0.83, $p<2.2e-16$) between the two sets of d-statistics, suggesting that expression changes associated with *SPOP*-mutation are largely shared with expression changes associated with high expression of BRD4 (Supplementary Fig. 5d). Collectively, these data suggest that SPOP mutations result in elevated BRD4 protein abundance that associates to prostate cancer progression.

To gain further insights into how SPOP governs BRD4 stability, we next examined the specific region(s) of BRD4 that interact(s) with SPOP (Fig. 3a). Interestingly, SPOP

specifically interacted with and promoted the degradation of the bromodomain region (1–470aa), but not other regions of BRD4 (Fig. 3b, c). A previous study has reported that well-characterized substrates of SPOP contain the Φ-Π-S-S/T-S/T consensus motif (where Φ is a nonpolar residue; Π is a polar residue; S is Serine; T is Threonine) [24]. Upon examination of the 1–470 amino acid sequence, we identified one evolutionally conserved putative SPOP binding motif or "degron" in all of BET family members (Fig. 3d). Strikingly, deletion of the identified degron (ΔD) led to an abolishment of BET proteins interaction with SPOP in cells and *in vitro* (Fig. 3e and Supplementary Fig. 6a–e). Moreover, the ΔD mutant of BET proteins was resistant to SPOP-mediated degradation (Fig. 3f and Supplementary Fig. 6f–h). As a result, the half-life of the ΔD-BRD4 mutant was significantly extended compared with WT-BRD4 (Fig. 3g, h and Supplementary Fig. 6i, j). Consistent with these findings, compared with WT-BRD4, the ΔD-BRD4 mutant was largely deficient in undergoing SPOP-mediated ubiquitination in cells and *in vitro* (Fig. 3i, j and Supplementary Fig. 6k). These results together indicate that the identified degron is the major motif that is responsible for SPOP-dependent regulation of BRD4 stability.

Interestingly, analysis of the COSMIC cancer database (http://cancer.sanger.ac.uk/cosmic) reveals a cancer patient-derived T295P (P is Proline) somatic mutation in the degron motif of BRD4, which may disrupt the canonical SPOP binding motif (Supplementary Fig. 6l). Indeed, we observed that the T295P-BRD4 mutant failed to interact with SPOP in cells (Supplementary Fig. 6m). As such, compared with WT-BRD4, the T295P-BRD4 mutant was resistant to SPOP-mediated ubiquitination and subsequent degradation (Supplementary Fig. 6n–q). These results indicate that the T295P mutation may stabilize and subsequently enhance the oncogenic role of BRD4 to promote tumorigenesis in part by evading SPOP-mediated degradation.

Next, we sought to explore the physiological roles of degron-mediated BRD4 degradation by SPOP in the prostate cancer setting. To this end, we found that ectopic expression of WT-BRD4, and to a greater extent, the non-degradable ΔD-BRD4 mutant, promoted cell proliferation and cell migration (Fig. 3l–n), supporting a possible oncogenic role for BRD4. More importantly, co-expression of SPOP suppressed WT-BRD4, but not ΔD-BRD4-mediated cell proliferation and cell migration (Fig. 3l–n), which is in large part due to the observation that ectopically expressed SPOP could efficiently promote the degradation of ectopically expressed WT-BRD4, but not ΔD-BRD4 (Fig. 3k) that is deficient in interacting with SPOP (Fig. 3e).

Notably, several BET inhibitors have been developed that mechanically disrupt the interaction of bromodomain proteins such as BRD4 with acetylated histones, leading to subsequent inhibition of transcription, cell growth and tumorigenesis [11,12]. Consistently, early clinical trials have shown that the BET inhibitors display promising therapeutic outcomes in patients [4]. However, more recent studies have identified mechanisms of resistance to BET inhibitors in leukemia and triple-negative breast cancer through elevation of Wnt/β-catenin signaling or hyper-phosphorylation of BRD4, respectively [13–15]. Therefore, it is crucial to investigate whether deficiencies in BRD4 degradation resulting from *SPOP* mutations may confer resistance to the BET inhibitors in prostate cancer. Interestingly, we observed that depletion of *BRD4* by shRNA or CRISPR-mediated

knockout could sensitize prostate cancer cells to BET inhibitors, JQ1 and I-BET (Fig. 4a, b and Supplementary Fig. 7a–e). In contrast, depletion of endogenous *SPOP* by shRNA or CRISPR-mediated knockout, which stabilizes BRD4 (Supplementary Fig. 7a), reduced JQ1 and I-BET sensitivity (Fig. 4a, b and Supplementary Fig. 7c–f) and inhibited JQ1-induced suppression of cellular migration (Supplementary Fig. 7g, h). Furthermore, additional depletion of *BRD4* re-sensitized *SPOP*-depleted cells to JQ1 (Fig. 4b), suggesting that *SPOP*-deficient cells acquired resistance to BET inhibitors largely due to elevation of BRD4 protein abundance.

In keeping with the notion that BET proteins are the primary drug targets of JQ1 [11], cells simultaneously depleted of endogenous BRD2/3/4 proteins displayed decreased proliferation rate and were less responsive to JQ1 treatment (Supplementary Fig. 7i–l). By contrast, stably expressing other SPOP substrates in *BRD4* knockout cells, such as AR and ERG, failed to restore JQ1 resistance (Supplementary Fig. 7m–o), indicating that all BET proteins, BRD4, BRD2 and BRD3, are likely JQ1 drug targets and their levels functionally contribute to JQ1 resistance in prostate cancer. Consistently, stable expression of SPOP-WT, but not the BRD4 interaction-deficient SPOP mutants in C4-2 or LNCaP cells conferred sensitivity to JQ1 and I-BET (Fig. 4c and Supplementary Fig. 8a–g), presumably due to their distinct behavior in dictating endogenous BET protein abundance in prostate cancer cells (Fig. 2e and Supplementary Fig. 3h). Moreover, compared with tumors expressing SPOP-WT, tumors expressing SPOP-mutant were resistant to JQ1 treatment in a xenograft mouse model (Fig. 4d–f and Supplementary Fig. 8h–j). Importantly, depletion of *BRD4,* but not other SPOP substrates such as *DEK, TRIM24* and *ERG,* could largely re-sensitize *SPOP*-deficient cells to JQ1 in C4-2 and 22Rv1 prostate cancer cells (Fig. 4g, h and Supplementary Fig. 8k–x).

Furthermore, in keeping with the notion that BRD4 protein levels dictate cellular sensitivity to BET inhibitors, we found that ectopic expression of WT-BRD4, or the non-degradable ΔD-BRD4 mutant at comparable levels, allowed cells to acquire resistance to JQ1 treatment (Supplementary Fig. 9a–b). More importantly, co-expression of SPOP could suppress WT-BRD4, but not ΔD-BRD4-mediated JQ1 resistance (Supplementary Fig. 9c–e). Consistently, in *BRD4* knockout C4-2 prostate cancer cells, reconstituted the non-degradable T295P-BRD4 mutant was relatively more stable than reconstituted WT-BRD4 (Supplementary Fig. 9f, g) in part due to its deficiency to interact with SPOP (Supplementary Fig. 6m), and depletion of *SPOP* in these cell lines elevated protein abundance of stably expressed WT-BRD4, but not T295P-BRD4 (Supplementary Fig. 9h). As a result, compared with cells reconstituted with T295P-BRD4, cells overexpressing WT-BRD4 were relatively more sensitive to JQ1 largely in a SPOP-dependent manner (Supplementary Fig. 9i). In keeping with these results, depletion of *SPOP* inhibited JQ1-induced cellular apoptosis largely in a BRD4-dependent manner (Fig. 4i and Supplementary Fig. 9j–l). On the other hand, ectopic expression of SPOP-WT, but not the prostate cancer-derived SPOP-W131G mutant, promoted cellular apoptosis upon JQ1 treatment, in part through destabilizing BRD4 (Fig. 4j and Supplementary Fig. 3h). Taken together, these data suggest that elevated protein levels of BRD4 might contribute to the observed resistance to BET inhibitors in prostate cancer cells.

To further investigate whether SPOP deficiency-induced accumulation of BRD4 contributes to JQ1 resistance in clinical models, we identified one prostate cancer patient-derived organoid harboring the W131R mutation in *SPOP*. Similar to other known prostate cancer-derived SPOP mutants, SPOP-W131R mutant also failed to promote ubiquitination and subsequent degradation of BET proteins largely due to impaired binding to BET proteins (Supplementary Fig. 9m–q). As a result, prostate cancer cells stably expressing SPOP-W131R mutant were resistant to JQ1 treatment (Supplementary Fig. 9r–t). Consistent with the results derived from cell culture model, compared with the SPOP-WT organoids, the SPOP-W131R organoid exhibited increased protein abundance of many SPOP substrates including BET proteins, SRC3 and TRIM24 (Fig. 4k), subsequently became more resistant to JQ1 treatment in both 2-D and 3-D culture conditions (Fig. 4l, m). More importantly, depletion of *BRD4* re-sensitized the SPOP-W131R organoids to JQ1 treatment (Fig. 4n, o), arguing that BRD4 protein abundance, but not the genetic background differences among WT and SPOP mutant organoids, accounts for the observed JQ1 resistance.

Having demonstrated a critical role for the SPOP/BRD4 signaling axis in mediating BET inhibitor resistance, we next explored how to target BRD4 in SPOP mutation prostate cancer cells to achieve better clinical outcomes. Recently, ligand-induced target protein degradation has emerged as a promising therapeutic strategy for cancer, such as phthalimides/Cereblon-mediated degradation of transcription factors, IKZF1 and IKZF3 [30,31]. To this end, dBET1, which is a hybrid compound of JQ1 and thalidomide, could specifically promote Cullin $4^{Cereblon}$-dependent degradation of BET proteins [32]. Notably, we found that similar to cellular response to other BET inhibitors, compared with parental C4-2 cells, *SPOP* knockout cells were relatively resistant, whereas *BRD4* knockout cells were more sensitive to dBET1 (Supplementary Fig. 10a), which is largely due to the fact that in *SPOP* knockout cells with elevated BRD4 protein abundance, dBET1 cannot efficiently promote the timely degradation of BRD4 to trigger cellular apoptosis in low dBET1 concentration (Supplementary Fig. 10b). Notably, we confirmed that, the expression of Cereblon was comparable in *SPOP* knockout cells and parental cells (Supplementary Fig. 10c). Moreover, dBET1 could efficiently promote BRD4 degradation in *Cereblon*-WT, but not *Cereblon* knockout 293FT and MMIS cells (Supplementary Fig. 10d, e). These results validate that cereblon is the major E3 ligase mediating dBET1-induced degradation of BRD4 protein. To further examine whether BRD4 protein abundance also dictates cellular dBET1 sensitivity, we treated the *SPOP* knockout cells with increased doses of dBET1. We found that dBET1 could gradually promote BRD4 degradation in high doses (Supplementary Fig. 10f). Moreover, in *SPOP* knockout cells, dBET1 could promote BRD4 degradation upon decreasing BRD4 abundance comparable to parental cells (Supplementary Fig. 10g).

Taken together, our study uncovers a critical tumor suppressive role of SPOP in prostate cancer by earmarking the BRD4 oncoprotein for timely destruction. Furthermore, we show that impairment of this signaling axis by either mutations at the E3 ligase (SPOP) level or the substrate (BRD4) level can prevent SPOP-mediated destruction of BRD4 by disrupting SPOP/BRD4 interaction, leading to stabilization and cooperation of BRD4 with various oncogenic transcription factors including AR and ERG to facilitate prostate tumorigenesis (Supplementary Fig. 2w). Notably, *SPOP* somatic mutations are mutually exclusive with ERG gene fusion [25], the most frequent genetic alteration event occurred in over 50% of

prostate cancer, which dominantly elevates both mRNA and protein levels of *ERG* and its downstream targets to promote cellular migration and invasion [33,34]. Our previous study demonstrated that *SPOP* deficiency, caused by either *SPOP* mutation or depletion of endogenous *SPOP*, led to a moderate increase of ERG protein levels to promote cellular migration [28]. Our current study suggests that in *SPOP*-deficient prostate cancer cells, elevation in BRD4 transcriptional co-activator might synergize with a moderate increase in ERG to favor cell migration and subsequent tumorigenesis. Moreover, our results also provide a possible molecular mechanism for BET inhibitor resistance in prostate cancer cells harboring *SPOP* mutations largely through stabilizing BET oncoproteins (Fig. 4p). We are also aware of that some SPOP-WT prostate cancer samples also exhibit high protein levels of BRD4 (Fig. 2n), indicating that other mechanisms, such as transcriptional regulation and genetic amplification, could also lead to BRD4 accumulation independent of *SPOP* mutation, which warrants for future in-depth study. Given the critical oncogenic role of BRD4 and high frequency of *SPOP* mutation in prostate cancer, our findings provide a molecular rationale for the clinical investigation of novel strategies to combat prostate cancer based on *SPOP* genetic status.

ONLINE METHODS

Cell culture

HEK293, HEK293T, HeLa, 293FT and mouse embryonic fibroblasts (MEFs) cells were maintained in DMEM medium supplemented with 10% FBS. LHMAR, MMIS, C4-2, 22Rv1 and LNCaP cells were cultured in RPMI 1640 medium with 10% FBS. $SPOP^{+/+}$ and $SPOP^{-/-}$ MEFs were obtained from Dr. Nicholas Mitsiades at Baylor College. *Cullin 4A* and *Cullin 4B* MEFs were gift of Dr. Pengbo Zhou at Weill Cornell Medical College. $293FT^{WT}$, $293FT^{CRBN-/-}$, $MMIS^{WT}$ and $MMIS^{CRBN-/-}$ cells were kind gift from Dr. William Kaelin at Dana Farber Cancer Institute. The human prostate cancer-derived organoids MSK-PCaX were cultured as described previously [35]. Cell transfection was performed as described previously [36]. No mycoplasma contamination was observed in these cell lines. Lentiviral shRNA virus packaging and subsequent infection of various cell lines were performed according to the protocol described previously [37]. BET inhibitors, including JQ1, I-BET, dBET1, were obtained from Dr. James E. Bradner group in Dana-Farber Cancer Institute. Cycloheximide (CHX) assays were performed as described previously [38].

Plasmids

GFP-BRD4, GFP-BRD2, GFP-BRD3, GFP-BRDT, HA-BRD4, Xpress-BRD4 truncations, Flag-Keap1, Flag-KLHL12 and Flag-KLHL37 were purchased from Addgene. Flag-BRD4 was obtained from Dr. Chris French at Brigham and Women's Hospital, Harvard Medical School. GST-BRD4 was generated by sub-cloning the BRD4 1-470 amino acid into pGEX-4T-1 vector. KLHL20 was gift of Dr. Ruey-Hwa Chen in Institute of Biological Chemistry, Academia Sinica (Taiwan). KLHL2 and KLHL3 were obtained from Dr. Shinichi Uchida at Tokyo Medical and Dental University. PLZF was gift of Dr. Junying Yuan at Harvard Medical School. Flag-COP1 and Flag-DET1 constructs were kind gift from Dr. William Kaelin at Dana-Farber Cancer Institute. Flag-AR and HA-AR constructs were from Dr. Shao-yong Chen at Beth Israel Deaconess Medical Center, Harvard Medical School.

SPOP related constructs were described previously [28]. Myc-Cullins constructs were described previously [38]. Various BRD4 mutants were generated using the QuikChange XL Site-Directed Mutagenesis Kit (Agilent) according to the manufacturer's instructions. Details of plasmid constructions are provided upon request.

shRNAs

shRNA vectors to deplete endogenous *SPOP* (shSPOP: TRCN0000122224, TRCN0000139181, TRCN0000145024), *ERG* (shERG:TRCN0000013913) and *BRD2/3* were purchased from Sigma. shRNA vectors to deplete endogenous *BRD4* were kind gifts from Dr. Takeshi Shimamura at Loyola University Chicago. shAR vectors were gift from Dr. Myles Brown at Dana-Farber Cancer Institute.

Antibodies

All antibodies were used at a 1:1000 dilution in 5% non-fat milk for western blot. Anti-ERG antibody [EPR3864 (2)] and (C-20) were purchased from Abcam and Santa Cruz, respectively. Anti-SPOP antibody (16750-1-AP), Anti-BRD2 (22236-1-AP) and anti-BRD3 (11859-1-AP) antibody were purchased from Proteintech. Anti-BRD4 antibody was purchased from Cell Signaling (13440) and Bethyl laboratories (A301-985A-M). Anti-Cullin 3 (2759), anti-GST (2625), anti-DEK (13962s), anti-SRC3 (2126), anti-Cleaved Caspase-3 (9664), anti-Cleaved PARP (5625), polyclonal anti-Myc-Tag antibody (2278) and monoclonal anti-Myc-Tag (2276) antibodies were purchased from Cell Signaling. Polyclonal anti-Flag antibody (F-2425), monoclonal anti-Flag antibody (F-3165, clone M2), anti-Tubulin antibody (T-5168), anti-Vinculin antibody (V-4505), anti-Flag agarose beads (A-2220), anti-HA agarose beads (A-2095), peroxidase-conjugated anti-mouse secondary antibody (A-4416) and peroxidase-conjugated anti-rabbit secondary antibody (A-4914) were purchased from Sigma. Monoclonal anti-HA antibody (MMS-101P) was purchased from Biolegend. Anti-GFP (8371-2) antibody was purchased from Clontech. Anti-Cullin 1 (SC-17775), anti-AR (N-20), anti-TRIM24/TIF1α (C-4), polyclonal anti-HA (SC-805) and anti-p27 (SC-528) were purchased from Santa Cruz. Anti-Xpress (46-0528) antibody was purchased from Invitrogen.

Immunoblots and immunoprecipitation

Cells were lysed in EBC buffer (50 mM Tris pH 7.5, 120 mM NaCl, 0.5% NP-40) supplemented with protease inhibitors (Complete Mini, Roche) and phosphatase inhibitors (phosphatase inhibitor cocktail set I and II, Calbiochem). The protein concentrations of lysates were measured by the Beckman Coulter DU-800 spectrophotometer using the Bio-Rad protein assay reagent. Same amounts of whole cell lysates were resolved by SDS-PAGE and immunoblotted with indicated antibodies. For immunoprecipitation, 1000 μg lysates were incubated with the indicated antibody (1–2 μg) for 3–4 hours at 4 °C followed by 1 hour incubation with Protein A sepharose beads (GE Healthcare). Immunoprecipitants were washed five times with NETN buffer (20 mM Tris, pH 8.0, 100 mM NaCl, 1 mM EDTA and 0.5% NP-40) before being resolved by SDS-PAGE and immunoblotted with indicated antibodies. Quantification of the immunoblot band intensity was performed with ImageJ software.

Real-time RT-PCR analyses

Total RNA was extracted using the RNeasy mini kit (Qiagen), and the reverse transcription reaction was performed using Power SYBR® Green PCR Master Mix (Thermo Fisher Scientific, 4367659). The real-time RT-PCR was performed with the 7500 Fast Real-time PCR system (ABI). Primers for BRD4 are 5′-AGCAGCAACAGCAATGTGAG-3′ and 5′-GCTTGCACTTGTCCTCTTCC-3′. Other primers for SPOP, AR and ERG target genes were described previously [28]. Data was shown as mean ± SD for three independent experiments.

In vitro ubiquitination assays

In vitro ubiquitination assays were performed as described previously [38]. Briefly, 293T cells were transfected with HA-SPOP, Myc-Cul3 and Myc-Rb×1 to purify SPOP/Cullin3/Rb×1 complex by HA immunoprecipitation. GST-BRD4-1-470 protein (wild-type and ΔD) was incubated with purified SPOP/Cullin3/Rb×1 complex together with E1, E2 (UbcH5a and UbcH3) and ubiquitin. The reactions were stopped by SDS sample buffer and resolved by SDS-PAGE for immunobloting.

In vivo ubiquitination assays

HeLa or HEK293 cells were transfected with HA-Ub and the desired constructs. Thirty-six hours post-transfection, cells were treated with 20 μM MG132 for 6 hours. Cells were lysed in denaturing buffer (1%SDS, 50 mM Tris, pH 7.5, 0.5 mM EDTA and 1 mM dithiothreitol). After incubation at 100 °C for 10 min, the lysate was sonicated and diluted 10 times with EBC lysis buffer and incubated with anti-HA-conjugated agarose beads (Sigma, mouse antibody) for 4 hours in 4 °C. Immunoprecipitants were washed five times with NETN buffer before resolved by SDS-PAGE and immublotted with indicated antibodies. *In vivo* His pull down ubiquitination assays were performed as described previously [28].

Migration assays

For cell migration assays, 3×10^4 to 1×10^5 cells were plated in a 8.0 μm 24-well plate chamber insert (Corning, 3422) with serum-free medium on the top of insert and 3T3 conditional medium containing 10% FBS at the bottom of the insert. Each sample was performed in triplicate. Cells were incubated for 24 hours and fixed with 4% paraformaldehyde for 15 min. After washed with PBS, cells on the top of the insert were scraped with a cotton swab. Cells adherent to the bottom were stained with 0.5% crystal violet blue for 15 min and then washed with ddH_2O. The positive staining cells were examined under microscope. Data was shown as mean ± SD from three independent experiments.

Cell viability assays

The indicated cell lines were seeded in 96-well (3×10^3 cells/well) plates and cultured in 100 ul medium containing 10% serum. After 24 hours, cells were treated with or without various concentrations of compounds in 50 μl medium for 24 to 48 hours and the cell viability was measured using the Cell Titer Glo (Promega) according to the manufacturer's instructions. The cell viability assay for the human prostate organoid MSK-PCaX cells were performed

as described previously [35, 39]. For 2-D culture, 5,000 organoids cells per well of a collagen coated 96-well cell culture were plated in 100 ul complete human media with vehicle (DMSO) control or JQ1 (10–3000 nM). Viable cells were counted using CellTiter-Glo (Promega) Luminescent Cell Viability Assay after 72 hours treatment. All cell viability experiments were conducted in triplicate. For 3-D culture, 5,000 organoids cells in 10 ul Matrigel per well were plated in 96-well cell culture plate. Viable cells under 3-day-treatment of 100 ul complete human media with vehicle (DMSO) control or JQ1 (10–3000 nM) were counted using CellTiter-Glo (Promega) Luminescent Cell Viability Assay. Data was shown as mean ± SD from three independent experiments.

Colony formation and soft agar assays

For the short-term colony formation assay, the cells were seeded in 6-well plates (1000–3000 cells/well) in medium and cultured for one to two weeks dependent on the size of the colony. Then the cells were fixed by methanol and acetic acid and stained with crystal violet and to count cell number. For the long-term soft agar assay, 2% melting Nobel agar was prepared and mixed with RPMI1640 to make the 0.4% and 0.8% agar in 50°C. 2 ml 0.8% Nobel agar was added in the bottom of the 6-well plate. 1×10^4 or 3×10^4 cells per well were mixed with 2 ml 0.4% agar and the mixture was added on the top of 0.8% agar. After routine culture for 4 to 6 weeks, colony numbers were stained with iodonitrotetrazolium chloride and counted. Data was shown as mean ± SD from three independent experiments.

Cell proliferation assays

For cell proliferation assays, the cells were seeded in 6-well plates (1×10^4 to 1×10^5 cells/well). At different time points, the cells were harvested and cell number was counted under the microscope. Or the cells were seeded in 96 well plates (1.5×10^3 cells/well). At the indicated time points, the cell proliferation was detected with MTS assay (Promega, G3530) according to the manufacturer's instructions. Data was shown as mean ± SD from three independent experiments.

Expression analysis in clinical samples of human prostate adenocarcinoma

Genomic alterations were identified by querying genomic data from Prostate Adenocarcinoma dataset of TCGA. Comprehensive data of 485 prostate adenocarcinoma cases were retrieved from the TCGA database (http://cancergenome.nih.gov/) regarding RNAseq gene expression (Illumina HiSeq RNASeqV2 Level 3.1.9.0). Annotations regarding *SPOP* mutation status were obtained from cBioPortal (http://www.cbioportal.org/) on the 06/29/2015 [40]. BRD4 mRNA expression levels were dichotomized into low and high expression categories using a model for classification based on finite normal mixture modeling (mclust 5.1 package, R 3.2.2). Differential gene expression was performed using two-class paired significance of microarray data (SAM 2.0 package, R 3.2.2) and genes considered differentially expressed when FDR < 0.05.

Immunohistochemistry (IHC)

BRD4 IHC staining was performed using the A301-985A antibody (Bethyl laboratories) in two sets of prostate cancer clinical samples. One set contains 66 SPOP wild type and 12

SPOP mutation prostate cancer samples as described previously [28]. The other set is a tissue microarray (TMA) of 369 analyzable, formalin-fixed paraffin-embedded tissue samples from the Institute of Pathology and Molecular Pathology, University Hospital Zurich, Switzerland [29]. Tumor stage and Gleason score of the cohort were assigned according to the International Union Against Cancer (UICC) and WHO/ISUP 2016 criteria [41]. The study was approved by the Cantonal Ethics Committee of Zurich (ZH-KEK-No. 2008-0025) and the associated methods were carried out in accordance with the approved guidelines.

Mouse xenograft assays

5×10^6 indicated C4-2 or 22Rv1 prostate cancer cells were suspended in 100 μl of RPMI 1640 medium and mixed with matrigel (Corning, 354234, 1:1) and injected into the flanks of male nude mice (10 mice for each group). Tumor size was measured every 2 days with a caliper and the tumor volume was determined with the formula: $L \times W2 \times 0.52$, where L is the longest diameter and W is the shortest diameter. At the end of the studies, mice were killed and in vivo solid tumors were dissected and weight. For JQ1 treatment assay, when the tumor volume reached 100–150 mm^3, xenografted mice were randomized and then received (6–7 mice for each group) vehicle or 50 mg/kg JQ1, 5 days a week. Tumor volume and weight were measured as mentioned above.

Statistics

The data (except animal data) were obtained from at least three times repeated experiments. No statistical method was used to predetermine sample size. Group variation was not estimated before experiments. The experiments were not randomized, except for the *in vivo* animal studies with mice, as described above. The number of mice per group was described in the corresponding figure legends and none of the animals was excluded from the experiment. Statistical associations between experimental groups were tested by two-tailed unpaired or paired Student's *t*-test, two-sided Fisher's exact test or Pearson's chi-squared test. Nonparametric Kaplan-Meier estimators were used to analyze overall, disease-specific and recurrence-free survival. Patients were censored at the time of their last clinical follow-up visit. Simultaneous 95% confidence bands were computed for the whole range of time values. Differences between survival estimates were evaluated by the log-rank test. The threshold for statistical significance was set to $p < 0.05$.

Data availability

Uncropped images for immunoblots and source data for statistics are provided in Supplementary Information section. All other relevant data are available from the corresponding author upon reasonable request.

Supplementary Material

Refer to Web version on PubMed Central for supplementary material.

Acknowledgments

We thank Fei Wu, Bin Wang, Naoe Taira Nihira, and Brian North for critical reading of the manuscript, and members of the Wei and Bradner laboratories for useful discussions. X.D. and J.G. are supported by a NRSA T-32

training grant. W.G. is supported by 1K99CA207867 from National Cancer Institute. D.L.B. is a Merck Fellow of the Damon Runyon Cancer Research Foundation (DRG-2196-14). P.J.W is funded in part by a H2020 grant of the European Comission (PrECISE) and a Research Grant of the University of Zurich, Switzerland. W.W. is an ACS research scholar. This work was supported in part by the NIH grants (W.W., GM094777 and CA177910).

References

1. Zeng L, Zhou MM. Bromodomain: an acetyl-lysine binding domain. FEBS Lett. 2002; 513:124–128. [PubMed: 11911891]
2. Wu SY, Chiang CM. The double bromodomain-containing chromatin adaptor Brd4 and transcriptional regulation. J Biol Chem. 2007; 282:13141–13145. [PubMed: 17329240]
3. Filippakopoulos P, Knapp S. The bromodomain interaction module. FEBS Lett. 2012; 586:2692–2704. [PubMed: 22710155]
4. Filippakopoulos P, Knapp S. Targeting bromodomains: epigenetic readers of lysine acetylation. Nat Rev Drug Discov. 2014; 13:337–356. [PubMed: 24751816]
5. Belkina AC, Denis GV. BET domain co-regulators in obesity, inflammation and cancer. Nat Rev Cancer. 2012; 12:465–477. [PubMed: 22722403]
6. Delmore JE, et al. BET bromodomain inhibition as a therapeutic strategy to target c-Myc. Cell. 2011; 146:904–917. [PubMed: 21889194]
7. Mertz JA, et al. Targeting MYC dependence in cancer by inhibiting BET bromodomains. Proc Natl Acad Sci U S A. 2011; 108:16669–16674. [PubMed: 21949397]
8. Asangani IA, et al. Therapeutic targeting of BET bromodomain proteins in castration-resistant prostate cancer. Nature. 2014; 510:278–282. [PubMed: 24759320]
9. French CA, et al. BRD4-NUT fusion oncogene: a novel mechanism in aggressive carcinoma. Cancer Res. 2003; 63:304–307. [PubMed: 12543779]
10. Crawford NP, et al. Bromodomain 4 activation predicts breast cancer survival. Proc Natl Acad Sci U S A. 2008; 105:6380–6385. [PubMed: 18427120]
11. Filippakopoulos P, et al. Selective inhibition of BET bromodomains. Nature. 2010; 468:1067–1073. [PubMed: 20871596]
12. Nicodeme E, et al. Suppression of inflammation by a synthetic histone mimic. Nature. 2010; 468:1119–1123. [PubMed: 21068722]
13. Fong CY, et al. BET inhibitor resistance emerges from leukaemia stem cells. Nature. 2015; 525:538–542. [PubMed: 26367796]
14. Rathert P, et al. Transcriptional plasticity promotes primary and acquired resistance to BET inhibition. Nature. 2015; 525:543–547. [PubMed: 26367798]
15. Shu S, et al. Response and resistance to BET bromodomain inhibitors in triple-negative breast cancer. Nature. 2016; 529:413–417. [PubMed: 26735014]
16. Holohan C, Van Schaeybroeck S, Longley DB, Johnston PG. Cancer drug resistance: an evolving paradigm. Nat Rev Cancer. 2013; 13:714–726. [PubMed: 24060863]
17. Gottesman MM. Mechanisms of cancer drug resistance. Annu Rev Med. 2002; 53:615–627. [PubMed: 11818492]
18. Housman G, et al. Drug resistance in cancer: an overview. Cancers (Basel). 2014; 6:1769–1792. [PubMed: 25198391]
19. Genschik P, Sumara I, Lechner E. The emerging family of CULLIN3-RING ubiquitin ligases (CRL3s): cellular functions and disease implications. EMBO J. 2013; 32:2307–2320. [PubMed: 23912815]
20. Vitari AC, et al. COP1 is a tumour suppressor that causes degradation of ETS transcription factors. Nature. 2011; 474:403–406. [PubMed: 21572435]
21. Jang MK, et al. The bromodomain protein Brd4 is a positive regulatory component of P-TEFb and stimulates RNA polymerase II-dependent transcription. Mol Cell. 2005; 19:523–534. [PubMed: 16109376]
22. Yang Z, et al. Recruitment of P-TEFb for stimulation of transcriptional elongation by the bromodomain protein Brd4. Mol Cell. 2005; 19:535–545. [PubMed: 16109377]

23. Wu SY, Lee AY, Lai HT, Zhang H, Chiang CM. Phospho switch triggers Brd4 chromatin binding and activator recruitment for gene-specific targeting. Mol Cell. 2013; 49:843–857. [PubMed: 23317504]
24. Zhuang M, et al. Structures of SPOP-substrate complexes: insights into molecular architectures of BTB-Cul3 ubiquitin ligases. Mol Cell. 2009; 36:39–50. [PubMed: 19818708]
25. Barbieri CE, et al. Exome sequencing identifies recurrent SPOP, FOXA1 and MED12 mutations in prostate cancer. Nat Genet. 2012; 44:685–689. [PubMed: 22610119]
26. Cancer Genome Atlas Research N. The Molecular Taxonomy of Primary Prostate Cancer. Cell. 2015; 163:1011–1025. [PubMed: 26544944]
27. Theurillat JP, et al. Prostate cancer. Ubiquitylome analysis identifies dysregulation of effector substrates in SPOP-mutant prostate cancer. Science. 2014; 346:85–89. [PubMed: 25278611]
28. Gan W, et al. SPOP Promotes Ubiquitination and Degradation of the ERG Oncoprotein to Suppress Prostate Cancer Progression. Mol Cell. 2015; 59:917–930. [PubMed: 26344095]
29. Zhong Q, et al. Image-based computational quantification and visualization of genetic alterations and tumour heterogeneity. Sci Rep. 2016; 6:24146. [PubMed: 27052161]
30. Lu G, et al. The myeloma drug lenalidomide promotes the cereblon-dependent destruction of Ikaros proteins. Science. 2014; 343:305–309. [PubMed: 24292623]
31. Kronke J, et al. Lenalidomide causes selective degradation of IKZF1 and IKZF3 in multiple myeloma cells. Science. 2014; 343:301–305. [PubMed: 24292625]
32. Winter GE, et al. DRUG DEVELOPMENT. Phthalimide conjugation as a strategy for in vivo target protein degradation. Science. 2015; 348:1376–1381. [PubMed: 25999370]
33. Kumar-Sinha C, Tomlins SA, Chinnaiyan AM. Recurrent gene fusions in prostate cancer. Nat Rev Cancer. 2008; 8:497–511. [PubMed: 18563191]
34. Rubin MA, Maher CA, Chinnaiyan AM. Common gene rearrangements in prostate cancer. J Clin Oncol. 2011; 29:3659–3668. [PubMed: 21859993]
35. Gao D, et al. Organoid Cultures Derived from Patients with Advanced Prostate Cancer. Cell. 2014; 159:176–187. [PubMed: 25201530]
36. Wei W, et al. Degradation of the SCF component Skp2 in cell-cycle phase G1 by the anaphase-promoting complex. Nature. 2004; 428:194–198. [PubMed: 15014503]
37. Boehm JS, Hession MT, Bulmer SE, Hahn WC. Transformation of human and murine fibroblasts without viral oncoproteins. Mol Cell Biol. 2005; 25:6464–6474. [PubMed: 16024784]
38. Inuzuka H, et al. Phosphorylation by casein kinase I promotes the turnover of the Mdm2 oncoprotein via the SCF(beta-TRCP) ubiquitin ligase. Cancer Cell. 2010; 18:147–159. [PubMed: 20708156]
39. Drost J, et al. Organoid culture systems for prostate epithelial and cancer tissue. Nature protocols. 2016; 11:347–358. [PubMed: 26797458]
40. Gao J, et al. Integrative analysis of complex cancer genomics and clinical profiles using the cBioPortal. Sci Signal. 2013; 6:pl1. [PubMed: 23550210]
41. Humphrey PA, Moch H, Cubilla AL, Ulbright TM, Reuter VE. The 2016 WHO Classification of Tumours of the Urinary System and Male Genital Organs-Part B: Prostate and Bladder Tumours. Eur Urol. 2016; 70:106–119. [PubMed: 26996659]

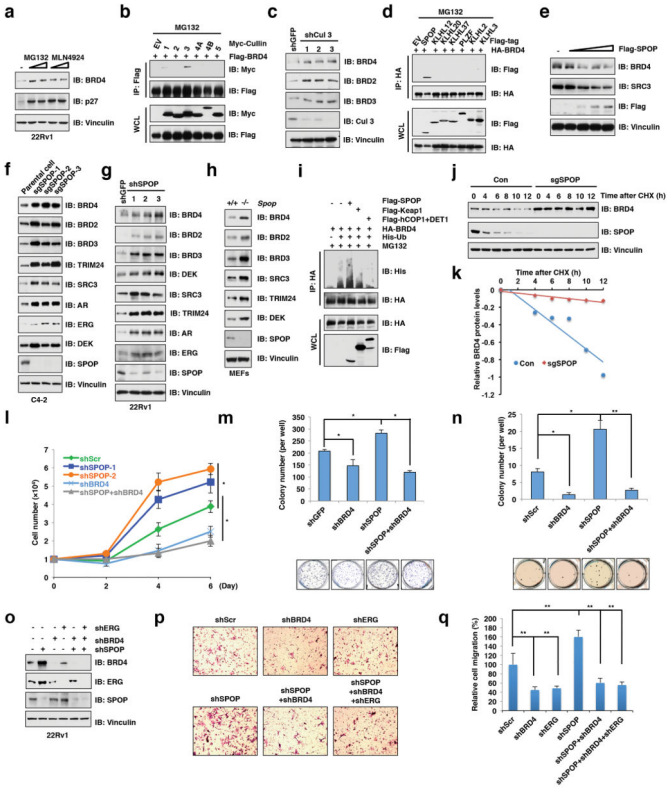

Figure 1. The Cullin 3^{SPOP} E3 ubiquitin ligase negatively regulates the stability of BET proteins

a. Immunoblot (IB) analysis of whole cell lysates (WCL) derived from 22Rv1 cells. Where indicated, MG132 or MLN4924 was added for 10 hours before harvesting the cells.

b. IB analysis of WCL and immunoprecipitates (IP) derived from 293 cells transfected with Flag-BRD4 and various Myc-tagged Cullin constructs. 30 hours post-transfection, cells were treated with 10 μM MG132 for 10 hours before harvesting.

c. IB analysis of WCL derived from 22Rv1 cells infected with the indicated lentiviral shRNAs. Infected cells were selected with 1 μg/ml puromycin for 72 hours to eliminate non-infected cells before harvesting.

d. IB analysis of WCL and IP derived from 293 cells transfected with HA-BRD4 and Flag-tagged BTB domain-containing protein constructs. 30 hours post-transfection, cells were treated with 10 μM MG132 for 10 hours before harvesting. EV, empty vector.

e. IB analysis of WCL derived from 22Rv1 cells transfected with increasing doses (0.5–3 μg) of Flag-SPOP.

f. IB analysis of WCL derived from C4-2 cells with *SPOP* knockout by the CRISPR technology. Parental C4-2 cells are used as the control.

g. IB analysis of WCL derived from 22Rv1 cells infected with the indicated lentiviral shRNAs. Infected cells were selected with 1 μg/ml puromycin for 72 hours to eliminate non-infected cells before harvesting.

h. IB analysis of WCL derived from *SPOP*$^{+/+}$ and *SPOP*$^{-/-}$ knockout mouse embryonic fibroblasts (MEFs).

i. IB analysis of WCL and IP derived from HeLa cells transfected with plasmids expressing the indicated proteins. 30 hours after transfection, cells were treated with the proteasome inhibitor MG132 (20 μM) for 6 hours before collecting.

j. *SPOP* knockout cells (sg*SPOP*) as well as parental C4-2 cells (Con) were treated with 100 μg/ml cycloheximide (CHX) for the indicated time period before harvesting. Equal amounts of WCL were immunoblotted with the indicated antibodies.

k. Quantification of the band intensities in **(j)**. BRD4 bands were normalized to vinculin, then normalized to the t = 0 time point.

l. The growth curve of 22Rv1 cell lines with depletion of *SPOP* and/or *BRD4*. shScr, Scramble. $*p < 0.05$, *t*-test.

m. Colony formation assays of 22Rv1 cell lines with depletion of *SPOP* and/or *BRD4*. $*p < 0.05$, *t*-test.

n. Soft agar assays of C4-2 cell lines with depletion of *SPOP* and/or *BRD4*. shScr, Scramble. $*p < 0.05$; $**p < 0.01$, *t*-test.

o. IB analysis of WCL derived from 22Rv1 cells infected with the indicated lentiviral shRNAs. shScr, Scramble. Infected cells were selected with 1 μg/ml puromycin for 72 hours to eliminate non-infected cells before harvesting.

p. Representative images of migrated 22Rv1 cells infected with indicated lentiviral shRNAs. shScr, Scramble.

q. Quantification of migrated cells in (**p**). Data was shown as mean ± SD for three independent experiments. $**p < 0.01$, *t*-test.

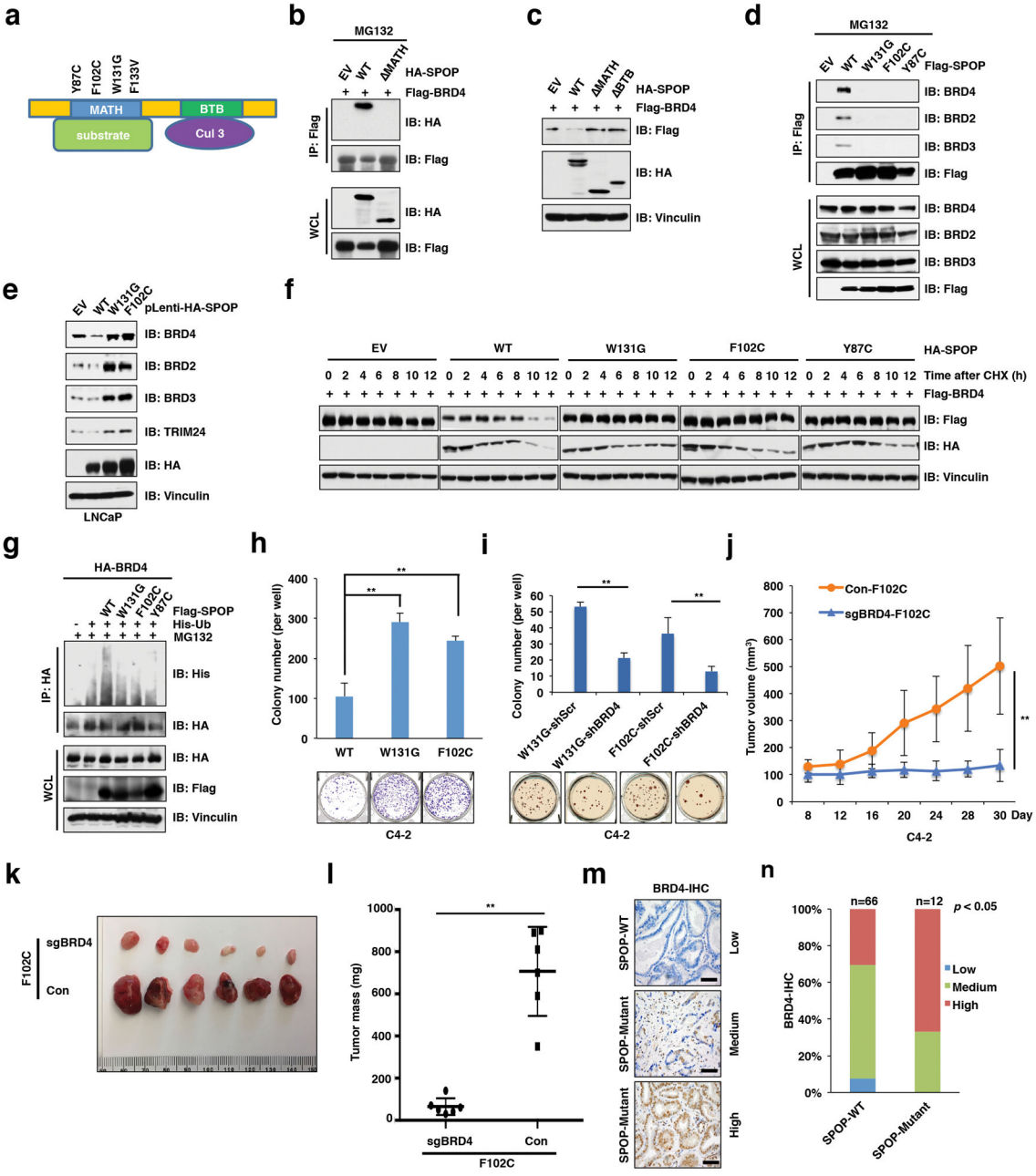

Figure 2. Prostate cancer-associated SPOP mutants promote prostate tumorigenesis largely by elevating protein levels of BET proteins

a. A schematic illustration of SPOP domains and prostate cancer-associated mutations.

b. Immunoblot (IB) analysis of whole cell lysates (WCL) and immunoprecipitates (IP) derived from 293 cells transfected with Flag-BRD4 and HA-SPOP-WT or deletion of MATH domain-SPOP constructs. 30 hours post-transfection, cells were treated with 10 μM MG132 for 10 hours before harvesting. EV, empty vector.

c. IB analysis of WCL derived from 293 cells transfected with indicated plasmids. EV, empty vector.

d. IB analysis of WCL and IP derived from 293 cells transfected with Flag-SPOP-WT or prostate cancer (PrCa)-associated SPOP mutants. Cells were treated with 10 μM MG132 for 10 hours before harvesting. EV, empty vector.

e. IB analysis of WCL derived from LNCaP cells stably expressing Flag-SPOP-WT or PrCa-associated SPOP mutants. EV, empty vector.

f. 293 cells transfected with Flag-BRD4 together with the indicated HA-SPOP expressing plasmids. 30 hours post-transfection, cells were treated with 100 μg/ml cycloheximide (CHX) for the indicated time period before harvesting. WCL were subjected to IB analysis. EV, empty vector.

g. *In vivo* ubiquitination assays of WCL and IP derived from HeLa cells transfected with plasmids expressing indicated proteins. 30 hours post-transfection, cells were treated with the proteasome inhibitor MG132 (20 μM) for 6 hours before cell collection.

h. Colony formation assays of C4-2 cell lines stably expressing SPOP-WT or PrCa-associated SPOP mutants. $^{**}p < 0.01$, *t*-test.

i. C4-2 cell lines stably expressing PrCa-associated SPOP mutants were infected with shScr (Scramble) or sh*BRD4* lentivirus. Infected cells were selected with 1 μg/ml puromycin for 72 hours to eliminate non-infected cells and used for colony formation assays. $^{**}p < 0.01$, *t*-test.

j–l. Parental or *BRD4* knockout C4-2 cells stably expressing SPOP-F102C were injected into nude mice (n=10 for each group). The *in vivo* tumor growth was monitored for indicated time period (**j**). Tumors were dissected and weighed (**k–l**). $^{**}p < 0.01$, *t*-test.

m. Representative images of primary prostate cancer patient samples stained for BRD4 by immunohistochemistry. Scale bar, 100 μm.

n. Statistical analysis of BRD4 expression in primary prostate cancer patient samples harboring *SPOP*-WT or *SPOP*-mutations. *p* value, Chi-squared test.

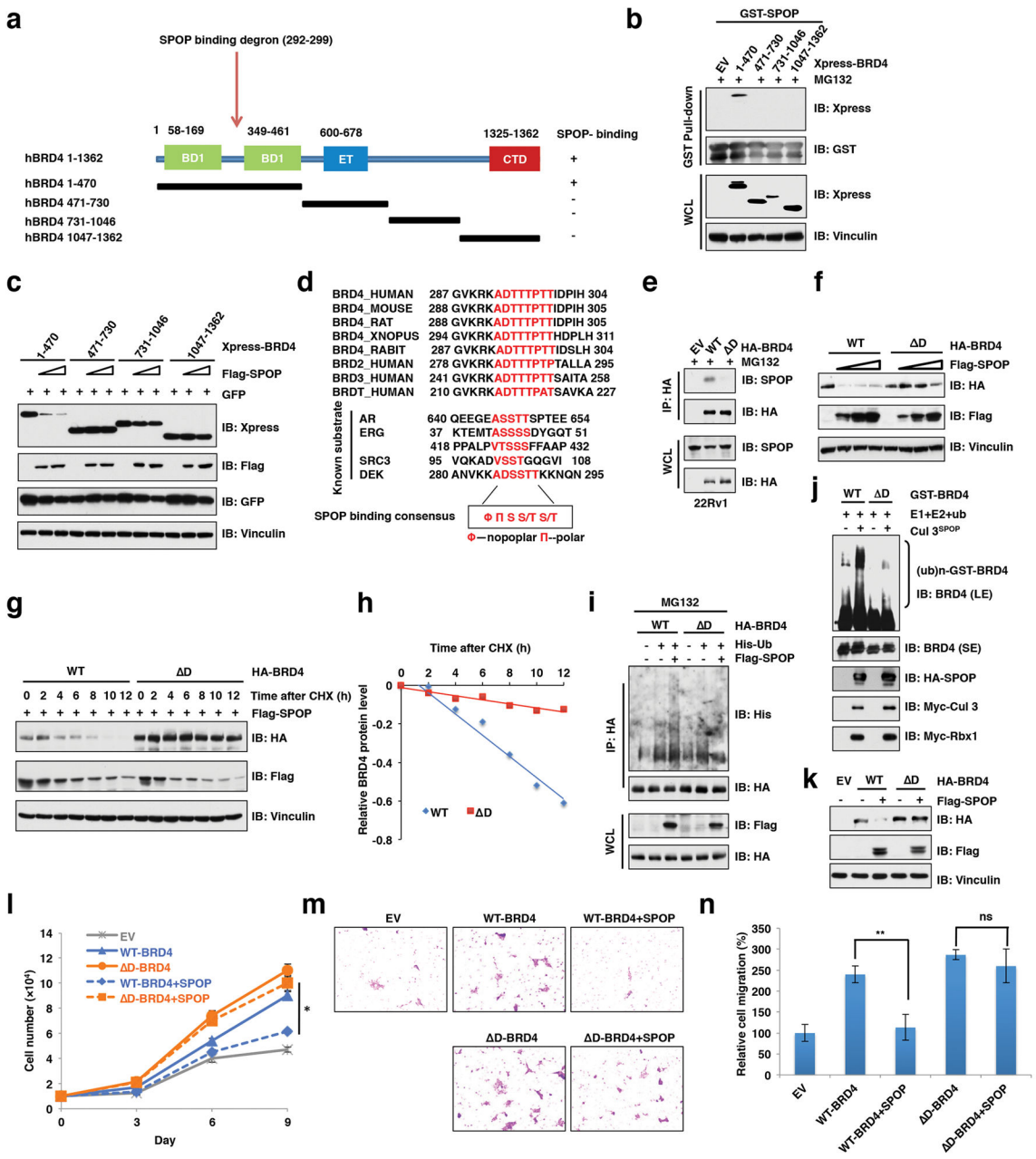

Figure 3. SPOP promotes ubiquitination and subsequent destruction of BET proteins in a degron-dependent manner

a. A schematic illustration of BRD4 domains and truncation of BRD4 constructs used in this study.

b. Immunoblot (IB) analysis of whole cell lysates (WCL) and GST pull down products. EV, empty vector.

c. IB analysis of WCL derived from 293 cells transfected with indicated Xpress-BRD4 truncated constructs different doses of Flag-SPOP expressing construct.

d. Sequence alignment of BET proteins with the SPOP binding motif (degron) in known SPOP substrates.

e. IB analysis of WCL and immunoprecipitates (IP) derived from 22Rv1 prostate cancer cells transfected with HA-WT-BRD4, ΔD-BRD4 constructs. 30 hours post-transfection, cells were treated with 10 μM MG132 for 10 hours before harvesting. EV, empty vector.
f. IB analysis of WCL derived from 293 cells transfected with indicated HA-BRD4 constructs with different doses of indicated Flag-SPOP expressing constructs.
g. 293 cells were transfected with indicated HA-BRD4 and Flag-SPOP expressing plasmids. 30 hours post-transfection, cells were treated with 100 μg/ml cycloheximide (CHX) for the indicated time period before harvesting. WCL were subjected to IB analysis.
h. Quantification of the band intensities in **(g)**. BRD4 bands were normalized to Vinculin, then normalized to the t = 0 time point.
i. *In vivo* ubiquitination assays of WCL and IP derived from HeLa cells transfected with plasmids expressing the indicated proteins. 30 hours after transfection, cells were treated with the proteasome inhibitor MG132 (20 μM) for 6 hours before cell collection.
j. The Cul 3^{SPOP} E3 ligase complex promotes BRD4 ubiquitination *in vitro*. Affinity-purified SPOP complexes were incubated with recombinant GST-BRD4 proteins, purified E1, E2 and ubiquitin. The ubiquitination reaction products were subjected to IB analysis with the anti-BRD4 antibody. LE, Longer Exposure; SE, Shorter Exposure.
k. IB analysis of WCL derived from 22Rv1 cells transfected with indicated constructs. EV, empty vector.
l. The growth curve of cells ectopically expressing SPOP and/or BRD4. EV, empty vector. $*p < 0.05$, *t*-test.
m–n. Representative images of migrated 22Rv1 cells transfected with indicated constructs in migration assay (**m**) and quantification of migrated cells (**n**). EV, empty vector. Data was shown as mean ± SD for three independent experiments. $**p < 0.01$, *t*-test; ns, non-significant.

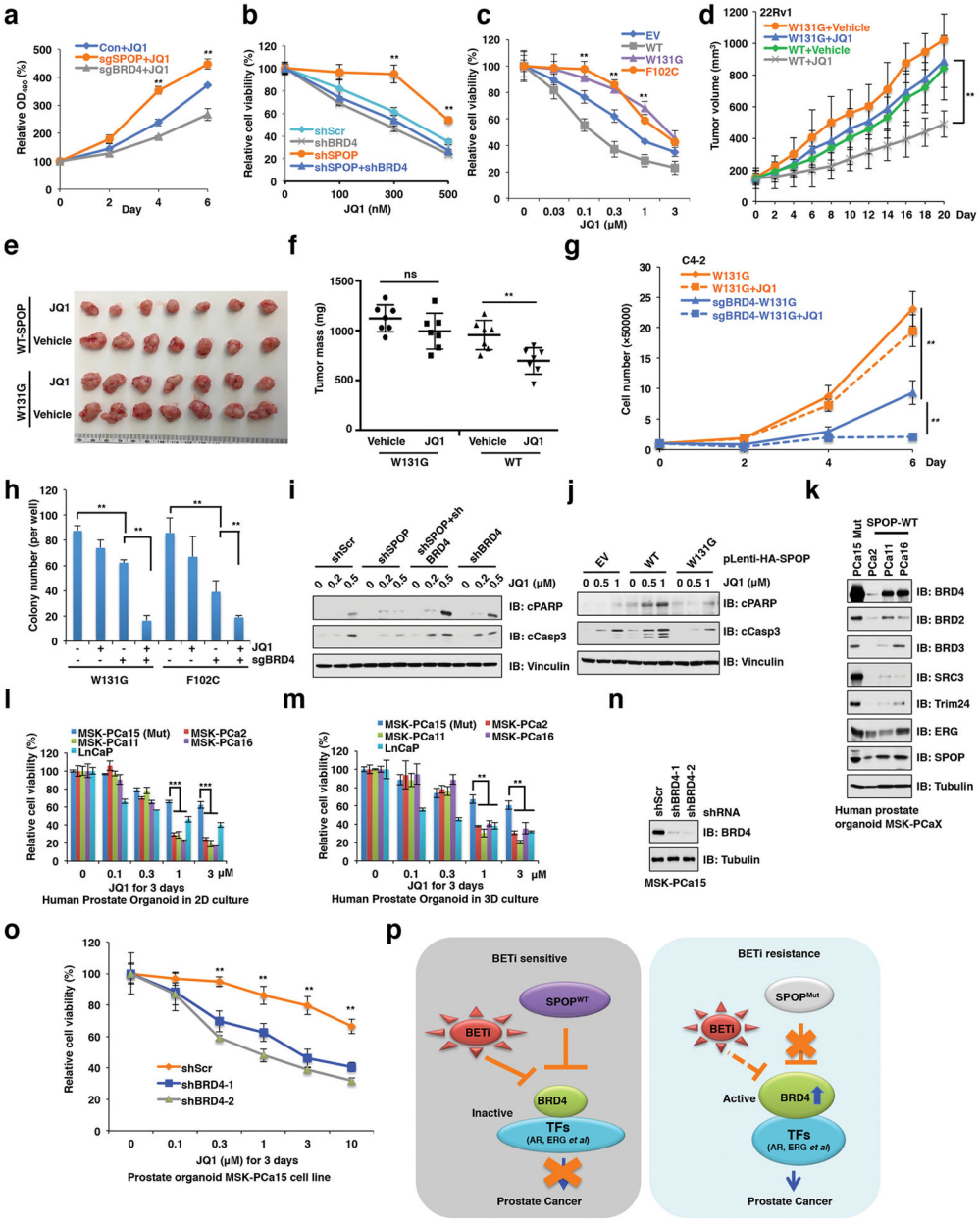

Figure 4. BRD4 protein abundance largely determines the resistance of *SPOP*-deficient prostate cancer cells to BET inhibitors

a. The growth curve of C4-2 cells with CRISPR-mediated *SPOP* knockout (sg*SPOP*) or *BRD4* knockout (sg*BRD4*) that were treated with JQ1 for the indicated time period. Parental C4-2 cells were used as control. $^{**}p < 0.01$, *t*-test.

b. Cell viability of C4-2 cells depleted for *SPOP* and/or *BRD4* treated with indicated concentration of JQ1 for 6 days. shScr, Scramble. $^{**}p < 0.01$, *t*-test.

c. Cell viability of C4-2 cells stably expressing SPOP-WT or PrCa-derived SPOP mutants that were treated with indicated concentration of JQ1. EV, empty vector. $^{**}p < 0.01$, *t*-test.

d–f. 22Rv1 cells stably expressing SPOP-WT or SPOP-W131G mutant were injected into nude mice (n=10 for each group) and grown until tumors reached a size of approximately 100 mm^3. Xenografted mice were randomized and then received (n=7 for each group) vehicle, 50 mg/kg JQ1, 5 days a week. *In vivo* tumor growth was monitored for indicated time period (**d**). Tumors were dissected and weighed (**e, f**). $^{**}p < 0.01$, *t*-test. ns, non-significant.

g. The growth curves of parental as well as CRISPR-mediated *BRD4* knockout (sg*BRD4*) of C4-2 cells stably expressing the SPOP-W131G mutant that were treated with JQ1 or vehicle. (10% cyclodextran in autoclaved water). $^{**}p < 0.01$, *t*-test.

h. Colony formation of parental as well as CRISPR-mediated *BRD4* knockout (sg*BRD4*) of C4-2 cells with stably expressing SPOP mutants that were treated with or without JQ1. $^{*}p < 0.05$, $^{**}p < 0.01$, *t*-test.

i–j. Immunoblot (IB) analysis of C4-2 cells depleting *SPOP* and/or *BRD4* (**i**) or ectopically expressing SPOP-WT or the SPOP-W131G mutant (**j**), treated with indicated doses of JQ1 for 24 hours before harvesting. shScr, Scramble; EV, empty vector.

k. IB analysis of whole cell lysates (WCL) derived from human prostate organoid MSK-PCax. MSK-PCa15 is the SPOP-W131R mutant organoid and MSK-PCa2, MSK-PCa11 and MSK-PCa16 are SPOP-WT organoids.

l–m. Cell viability of human prostate MSK-PCax organoids in 2-D (l) and 3-D (m) culture conditions that were treated with indicated concentration of JQ1 for 4 days. $^{**}p < 0.01$, $^{***}p < 0.001$, *t*-test.

n. IB analysis of WCL derived from human prostate MSK-PCa15 (SPOP-W131R) organoids infected with lentiviral sh*BRD4*. Infected cells were selected with 0.5 μg/ml puromycin for 48 hours to eliminate non-infected cells before harvesting. shScr, Scramble.

o. Cell viability of human prostate organoids MSK-PCa15 depleted for *BRD4* in 2-D culture conditions treated with indicated concentrations of JQ1 for 72 hours. shScr, Scramble. $^{**}p < 0.01$, *t*-test.

q. A schematic illustration of the proposed mechanism through which SPOP mutations lead to BET inhibitor (BETi) resistance in the prostate cancer setting. TFs, transcription factors.